Int J Theor Phys (2008) 47: 1028–1038
DOI 10.1007/s10773-007-9531-y

Possible Critical Orientations of Interacting Composite Particles

Kwang-Hua W. Chu

Received: 13 June 2007 / Accepted: 17 August 2007 / Published online: 18 September 2007
© Springer Science+Business Media, LLC 2007

Abstract We obtain possibly valuable information about the phase diagram linked to the critical orientations for composite matter subjected to interactions at high fermion as well as boson number density but low temperature, which is not easily accessible to experiments. Our results qualitatively resemble those proposed before by using other theories once we can calibrate our results by tuning the critical orientation and the rarefaction measure (relevant to the temperature).

Keywords Fundamental particles · Pauli exclusion principle · Acoustic analog

1 Introduction

Although the recent close inspection by the Hubble Space Telescope of the area of interest (cf. [55]) appears to indicate that no string is present (see, e.g. [56]), the possibility remains that strings may be found through other types of observation in the Universe. Note that when two ordinary cosmic strings (please see the review by Hindmarsh and Kibble [36] or Davis [24] for the details) intersect, they normally 'intercommute', or exchange partners. Recent study (cf. [23]) of the interaction of a pair of straight strings instead show that there are important kinematical constraints implying that such intercommuting is impossible for strings that meet with very high relative velocity. The limit depends on the angle at which the strings meet and on the ratios of the string tensions. Thus, the orientation effect is important to the dynamics (and thermodynamics) of systems of straight strings although this study is already rather difficult (cf. Polchinski [54] or [57]) even considering only the general collision between two straight strings (cf. [58]). This is one motivation for our present attempt.

We noticed that some researchers represented baryons as pieces of open string connected at one common point (cf. [61]). Thus, as a preliminary investigation, the collision of system of rigid straight strings is also of academic interest. Here, for simplicity, we only consider

K.-H.W. Chu (✉)
College of Physics and Information Engineering, Hebei Normal University, Shijiazhuang 050016, China
e-mail: khwchu@126.com

collisions of system of straight (long-enough) strings (with the same tensions) which are confined to move only two-dimensionally (the projection of each string lying within the plane which is perpendicular to the string axis). To make further approximation as the problem is still of higher dimension (considering the dimension of strings), we only consider the projection of each string into the plane perpendicular to the axis of the straight string: a point particle and associate it with an (intrinsic) orientation when these system of particles collide with each other (when strings collide with a relative angle, they may be cut once at the collision and connected at the different ends. This is called reconnection (or recombination, inter-commutation; cf. [32] or [5]) but it resembles that of two indistinguishable particles collide and then depart from the view point (in the direction of the string axis) lying far away from these strings or projections at the plane perpendicular to their axes). We will not consider the collisions of three straight (longer enough) strings (cf. [23]) here.

The only place in the universe where we expect sufficiently high densities and low temperatures is compact stars, also known as 'neutron stars', since it is often assumed that they are made primarily of neutrons (for a recent review, see [42]). A compact star is produced in a supernova. As the outer layers of the star are blown off into space, the core collapses into a very dense object. In a broader perspective, neutron stars and heavy-ion collisions provide access to the phase diagram of matter at extreme densities and temperatures, which is basic for understanding the very early Universe and several other astrophysical phenomena. These range from nuclear processes on the stellar surface to processes in electron degenerate matter at subnuclear densities to boson condensates and the existence of new states of baryonic matter such as color superconducting quark matter at supernuclear densities. More than that, according to the strange matter hypothesis strange quark matter could be more stable than nuclear matter, in which case neutron stars should be largely composed of pure quark matter possibly enveloped in thin nuclear crusts. Neutron stars and white dwarfs are in hydrostatic equilibrium, so at each point inside the star gravity is balanced by the degenerate particle pressure, as described mathematically by the Tolman–Oppenheimer–Volkoff equation [53, 62].

It is often stressed that there has never been a more exciting time in the overlapping areas of nuclear physics, particle physics, and relativistic astrophysics than today (cf. [35]). Neutron stars are dense, neutron-packed remnants of massive stars that blew apart in supernova explosions. They are typically about twenty kilometers across and spin rapidly, often making several hundred rotations per second. Many neutron stars form radio pulsars, emitting radio waves that appear from the Earth to pulse on and off like a lighthouse beacon as the star rotates at very high speeds. Depending on star mass and rotational frequency, gravity compresses the matter in the core regions of pulsars up to more than ten times the density of ordinary atomic nuclei, thus providing a high pressure environment in which numerous subatomic particle processes compete with each other.

The most spectacular ones stretch from the generation of hyperons and baryon resonances to quark deconfinement to the formation of boson condensates. There are theoretical suggestions of even more exotic processes inside neutron stars, such as the formation of absolutely stable strange quark matter, a configuration of matter more stable than the most stable atomic nucleus, ^{62}Ni. Instead these objects should be named nucleon stars, since relatively isospin symmetric nuclear matter-in equilibrium with condensed K^- mesons-may prevail in their interiors, hyperon stars if hyperons (Σ, Λ, Ξ, possibly in equilibrium with the Δ resonance) become populated in addition to the nucleons, quark hybrid stars if the highly compressed matter in the centers of neutron stars were to transform into u, d, s quark matter, or strange stars if strange quark matter were to be more stable than nuclear matter. Of course, at present one does not know from experiment at what density the expected phase

transition to quark matter occurs. Neither do lattice Quantum ChromoDynamical (QCD) simulations provide a conclusive guide yet. From simple geometrical considerations it follows that, for a characteristic nucleon radius of $r_N \sim 1$ fm, nuclei begin to touch each other at densities of $\sim(4\pi r_N^3/3))^{-1} \approx 0.24$ fm^3, which is less than twice the baryon number density of ordinary nuclear matter, $\rho_0 = 0.16$ fm^3 (energy density $\epsilon_0 = 140$ MeV/fm^3). Depending on the rotational frequency and stellar mass, such densities are easily surpassed in the cores of neutron stars so gravity may have broken up the neutrons (n) and protons (p) in the centers of neutron stars into their constituents. The phase diagram of quark matter, expected to be in a color superconducting phase, is very complex [1, 35], da Silva and Hadjimichef [25]. At asymptotic densities the ground state of QCD with a vanishing strange quark mass is the color-flavor locked (CFL) phase. This phase is electrically charge neutral without any need for electrons for a significant range of chemical potentials and strange quark masses.

Quite recently McLaughlin et al. [50] searched for radio sources that vary on much shorter timescales. They found eleven objects characterized by single, dispersed bursts having durations between 2 and 30 ms. The average time intervals between bursts range from 4 min to 3 h with radio emission typically detectable for < 1 s per day. From an analysis of the burst arrival times, they have identified periodicities in the range 0.4–7 s for ten of the eleven sources, suggesting origins in rotating neutron stars. Meanwhile as all pulsars from which giant pulses have been detected appear to have high values of magnetic field strength at their light cylinder radii (cf. [38]). While the Crab pulsar has a magnetic field strength at the light cylinder of 9.3×10^5 G, this value ranges from only 3 to 30 G for these sources, suggesting that the bursts originate from a different emission mechanism. They therefore concluded that these sources represent a previously unknown population of bursting neutron stars, which they call rotating radio transients (RRATs). These interesting new observations make us to investigate the rotation (e.g., it is still controversial how much angular momentum the iron cores have before the onset of the gravitational-collapse) as well as Pauli-blocking effects [2, 37] in compact stars considering the possible phase diagram. This is another motivation for our present study here.

In present approach (following equations (2) and (3) below) the Uehling–Uhlenbeck collision term [18–20, 26, 63, 64], which could describe the collision of a gas of dilute hard-sphere Fermi- or Bose-particles by tuning a parameter γ: a Pauli-blocking factor (or γf with f being a normalized (continuous) distribution function giving the number of particles per cell) is adopted together with a free-orientation θ (which is related to the relative direction of scattering of particles w.r.t. to the normal of the propagating plane-wave front) into the quantum discrete kinetic model [18–20, 64] which can be used to obtain dispersion relations of plane (sound) waves propagating in different-statistic gases (of particles). We then study the critical behavior based on the acoustical analog [15–17, 49] which has been verified before. The possible phase diagram (as the orientation is changed) we obtained resemble qualitatively those proposed before (cf. [1]). We firstly introduce in brief previous QCD transport theories since our results might be calibrated with those obtained via QCD. To satisfy the generalized Pauli exclusion principle, researchers make the further assumption that each of the quarks (say, u-, d-, and s-quark) comes in three varieties that are distinguished by a further feature: *color*. Thus, the basis of SU(3) color symmetry scheme and quantum chromodynamics (QCD) forms $(\mathrm{SU}(3)_c$ is another SU(3) group called the *color* group which is presumed to not experience spontaneous symmetry breaking and so the gluons remain massless).

Note that as the temperature T of the quark-gluon plasma is much greater than the QCD scale parameter Λ_{QCD}, the hard modes, i.e. those with momenta of the order of T or larger, are weakly interacting and they can be described within perturbative QCD (cf. [22]). The

dynamics of the soft sector, however, remains non-perturbative even at arbitrarily large temperature (cf. [30]), as signaled by severe infrared divergences (cf. [44]). Then, one has to refer to effective theories to get an insight into the soft mode dynamics. Such theories, see e.g. [9–11], can be derived from QCD by integrating out the hard modes, but constructing them is by far not a simple task. Consequently, one often relies on more or less heuristic approaches, usually exploiting a semi-classical or classical field approximation because the occupation numbers of the soft gluonic modes are large. A very natural effective approach is provided by the kinetic theory, where the hard modes are treated as (quasi-)particles while the soft gluonic ones contribute to the chromodynamic mean field. The transport theory has been formulated in two versions. The first one treats the color degrees of freedom as a classical continuous variable which, as position or momentum, evolves in time. A starting point of the theory are the Wong equations (cf. [66]), which describe a classical particle that interacts with the chromodynamic field due to the color charge. Then, one immediately gets the Liouville and the transport equations [33, 34] of a many-body quark-gluon system. The physical content of the theory is rather transparent and numerous results, for example transport coefficients, can be easily obtained. Even the simplest collisionless transport equations, where the dissipation phenomena are neglected, provides a surprisingly rich dynamics. The transport theory with the classical color became really reliable when the theory was found (cf. [40]) to reproduce the QCD hard-thermal-loop dynamics [12, 60]. It was further established (cf. [45]) that the theory supplemented by the collision terms, obtained integrating out soft around the mean fields, agrees with the QCD effective approaches (cf. [3]).

In the second version of the QCD transport theory (cf. [65]), the color charges are represented, in full accordance with QCD, by a matrix structure of the distribution function. The Vlasov transport equation of quarks was derived by Elze et al. [28] directly from QCD, by analyzing the motion of quantum quarks in the classical chromodynamic field. The gluon transport equation was found (cf. [29]), by splitting the gluon field into the mean field and the contribution representing the particle excitations. It was further observed by Mrówczyński [51] that the quark and gluon transport equations are formally identical when the first one is written in the fundamental representation and the second one in the adjoint representation. Then, the quark and gluon distribution functions are $N_c \times N_c$ and $(N_c^2 - 1) \times (N_c^2 - 1)$ matrices, respectively, for the SU(N_c) gauge group. In quasi-equilibrium, the matrix transport theory was proved by Blaizot and Iancu [6] to be fully equivalent to the QCD hard-loop approach. The kinetic approach, which can be treated as a local presentation of the non-local hard-loop action, is particularly useful to study the collective excitations of the quark-gluon plasma. More recently, the quasi-equilibrium kinetic equations have been derived beyond the collisionless limit (cf. [7]) and the QCD effective theories have again been correctly reproduced.

A natural question that arises is where the agreement between the kinetic theory, either with the classical color or in the matrix form, and the finite temperature diagrammatic approach breaks down. Laine and Manuel [43] later on studied the kinetic theory with the classical color and it was found to reproduce the g^4 contribution to the effective action only in the limit of high-dimensional color representations. Thus, the limitations of the classical approach have been explicitly determined. Quite recently Manuel and Mrówczyński [47] looked for the solutions of the transport equations for quarks and gluons interacting with a chromodynamic mean field. The system is assumed to be translation invariant in one or more space-time directions. Thus, their considerations hold, in particular, for static and for homogeneous systems. In fact, similar approaches (as well as our present one: Uehling–Uhlenbeck collision forms, equations (2) and (3) below) have been applied to some QCD transport problems. These observations together with our present verified approaches: combining Uehling–Uhlenbeck equations (cf. [18–21, 64]) with acoustic analog

(cf. [15–17, 21]), as we believe, could provide valuable information about orientation effects (might be relevant to the strong magnetic field or external confined potentials) to the phase diagram of nuclear matter (related to the thermodynamics but not non-equilibriuym transport). The preliminary results we present here can also tell us: how far the limits of the Uehling–Uhlenbeck approach can be extended to non-Abelian kinetic one.

2 Theoretical Formulations

The velocities of particles (or projections of system of rigid straight (long-enough) strings onto the plane perpendicular to the string-axis) are restricted to, e.g., $\mathbf{u}_1, \mathbf{u}_2, \ldots, \mathbf{u}_p$, p is a finite positive integer. The discrete number densities of particles are denoted by $N_i(\mathbf{x}, t)$ associated with the velocities $\mathbf{u}_i$ at point $\mathbf{x}$ and time t. If only nonlinear binary collisions and the evolution of N_i are considered, we have

$$\frac{\partial N_i}{\partial t} + \mathbf{u}_i \cdot \nabla N_i = F_i \equiv \frac{1}{2} \sum_{j,k,l} (A_{kl}^{ij} N_k N_l - A_{ij}^{kl} N_i N_j), \quad i \in \Lambda = \{1, \ldots, p\}, \tag{1}$$

where (i, j) and (k, l) $(i \neq j$ or $k \neq l)$ are admissible sets of collisions (cf. [18–21, 64]). Here, the summation is taken over all $j, k, l \in \Lambda$, where A_{kl}^{ij} are nonnegative constants satisfying $A_{kl}^{ji} = A_{kl}^{ij} = A_{lk}^{ij}$, $A_{kl}^{ij}(\mathbf{u}_i + \mathbf{u}_j - \mathbf{u}_k - \mathbf{u}_l) = 0$, and $A_{kl}^{ij} = A_{ij}^{kl}$. The conditions defined for the discrete velocities above require that there are elastic, binary collisions, such that momentum and energy are preserved, i.e., $\mathbf{u}_i + \mathbf{u}_j = \mathbf{u}_k + \mathbf{u}_l$, $|\mathbf{u}_i|^2 + |\mathbf{u}_j|^2 = |\mathbf{u}_k|^2 + |\mathbf{u}_l|^2$, are possible for $1 \leq i, j, k, l \leq p$. We note that, the summation of N_i $(\sum_i N_i)$: the total discrete number density here is related to the macroscopic density: $\rho\ (= m_p \sum_i N_i)$, where m_p is the mass of the particle [18–21, 64].

Together with the introducing of the Uehling–Uhlenbeck collision term (cf. [18–21, 64]):

$$F_i = \sum_{j,k,l} A_{kl}^{ij} [N_k N_l (1 + \gamma N_i)(1 + \gamma N_j) - N_i N_j (1 + \gamma N_k)(1 + \gamma N_l)], \tag{2}$$

into (1), for $\gamma < 0$ (normally, $\gamma = -1$), we can then obtain a quantum discrete kinetic equation for a gas of Fermi-particles; while for $\gamma > 0$ (normally, $\gamma = 1$) we obtain one for a gas of Bose-particles, and for $\gamma = 0$ we recover (1).

Considering binary collisions only, from equation above, the model of quantum discrete kinetic equation for Fermi or Bose gases proposed before is then a system of $2n(= p)$ semilinear partial differential equations of the hyperbolic type:

$$\frac{\partial}{\partial t} N_i + \mathbf{v}_i \cdot \frac{\partial}{\partial \mathbf{x}} N_i = \frac{cS}{n} \sum_{j=1}^{2n} N_j N_{j+n} (1 + \gamma N_{j+1})(1 + \gamma N_{j+n+1})$$

$$- 2cS N_i N_{i+n} (1 + \gamma N_{i+1})(1 + \gamma N_{i+n+1}), \quad i = 1, \ldots, 2n, \tag{3}$$

where $N_i = N_{i+2n}$ are unknown functions, and $\mathbf{v}_i = c(\cos[\theta + (i-1)\pi/n], \sin[\theta + (i-1)\pi/n])$; c is a reference velocity modulus and is the same order of the sound speed in the absence of scatters), θ is the free orientation starting from the positive x-axis to the u_1 direction and could be related to the external strong magnetic field or confined potential or parameter relevant to the global internal symmetry, S is an effective collision cross-section for the collision system.

As we adopt the acoustic analog approach, so we shall derive the dispersion relations for plane waves propagating inside system of colliding particles (or projections of system of rigid straight (long-enough) strings onto the plane perpendicular to the string-axis) from above equations. Note that the passage of the plane (sound) wave will cause a small departure from an equilibrium state and result in energy loss owing to internal friction and heat conduction, we then linearize above equations around a uniform equilibrium state (particles' number density: N_0) by setting $N_i(t,x) = N_0\ (1 + P_i(t,x))$, where P_i is a small perturbation. After some similar manipulations (please refer to [15, 17] or [21]), with $B = \gamma N_0 < 0$, which gives or defines the (proportional) contribution from the Fermi gases (if $\gamma < 0$, e.g., $\gamma = -1$) or the Bose gases ($B > 0$, if $\gamma > 0$, e.g., $\gamma = 1$), we then have

$$\left[\frac{\partial^2}{\partial t^2} + c^2\cos^2\left[\theta + \frac{(m-1)\pi}{n}\right]\frac{\partial^2}{\partial x^2} + 4cSN_0(1+B)\frac{\partial}{\partial t}\right]D_m = \frac{4cSN_0(1+B)}{n}\sum_{k=1}^{n}\frac{\partial}{\partial t}D_k, \tag{4}$$

where $D_m = (P_m + P_{m+n})/2$, $m = 1, \ldots, n$, since $D_1 = D_m$ for $1 = m \pmod{2n}$.

We are ready to look for the solutions in the form of plane wave $D_m = a_m \exp i(kx - \omega t)$, $(m = 1, \ldots, n)$, with $\omega = \omega(k)$. This is related to the dispersion relations of 1D (forced) plane wave propagation in Fermi or Bose gases. So we have

$$\left(1 + ih(1+B) - 2\lambda^2\cos^2\left[\theta + \frac{(m-1)\pi}{n}\right]\right)a_m - \frac{ih(1+B)}{n}\sum_{k=1}^{n}a_k = 0, \quad m = 1, \ldots, n, \tag{5}$$

where

$$\lambda = kc/(\sqrt{2}\omega), \qquad h = 4cSN_0/\omega \propto 1/K_n,$$

where h is the rarefaction parameter of the gas; K_n is the Knudsen number which is defined as the ratio of the mean free path of gases to the wave length of the plane (sound) wave.

3 Results and Discussions

We firstly introduce the concept of acoustical analog [15–17, 49] in brief. In a mesoscopic system, where the sample size is smaller than the mean free path for an elastic scattering, it is satisfactory for a one-electron model to solve the time-independent Schrödinger equation: $-(\hbar^2/2m)\nabla^2\psi + V'(\vec{r})\psi = E\psi$ or (after dividing by $-\hbar^2/2m$) $\nabla^2\psi + [q^2 - V(\vec{r})]\psi = 0$, where q is an (energy) eigenvalue parameter, which for the quantum-mechanic system is $\sqrt{2mE/\hbar^2}$. Meanwhile, the equation for classical (scalar) waves is $\nabla^2\psi - (\partial^2\psi/c^2\,\partial t^2) = 0$ or (after applying a Fourier transform in time and contriving a system where c (the wave speed) varies with position $\vec{r}$) $\nabla^2\psi + [q^2 - V(\vec{r})]\psi = 0$, here, the eigenvalue parameter q is ω/c_0, where ω is a natural frequency and c_0 is a reference wave speed. Comparing the time dependencies one gets the quantum and classical relation $E = \hbar\omega$. The localized state (associated with a corresponding critical orientation) could thus be determined via E or the rarefaction parameter (h) which is related to the ratio of the collision frequency and the wave frequency.

The complex spectra ($\lambda = \lambda_r + \mathrm{i}\ \lambda_i$; the real part $\lambda_r = k_r c/(\sqrt{2}\omega)$: sound dispersion, a relative measure of the sound or phase speed; the imaginary part $\lambda_i = k_i c/(\sqrt{2}\omega)$: sound attenuation or absorption) could be obtained from the complex polynomial equation above. Here, the Pauli-blocking parameter (B) could be related to the occupation number of different-statistic particles of gases (cf. [21, 64]). To examine the critical region possibly tuned by the Pauli-blocking measure $B = \gamma N_0$ and the free orientation θ, as evidenced from previous Boltzmann results (cf. [16, 17]): $\lambda_i = 0$ for cases of $\theta = \pi/4$ (or $B = -1$), we firstly check those spectra near $\theta = 0$, say, $\theta = 0.005$ and $\theta = \pi/4 \approx 0.7854$, say, $\theta = 0.78535$ for a B-sweep (B decreases from 1 to -1), respectively. Note that, as the free-orientation θ is not zero, there will be two kinds of propagation of the disturbance wave: sound and diffusion modes (cf. [21, 48]). The latter (anomalous) mode has been reported in Boltzmann gases (cf. [15, 17]) and is related to the propagation of entropy wave which is not used in the acoustical analog here. The absence of (further) diffusion (or maximum absorption) for the sound mode at certain state (h, corresponding to the inverse of energy E; cf. Chu in Ref. [15]) is classified as a localized state (resonance occurs) based on the acoustical analog [15–17]. The state of decreasing h might, in one case [27], correspond to that of T (absolute temperature) decreasing as the mean free path is increasing (density or pressure decreasing).

We have observed the max. λ_i (absorption of sound mode, relevant to the localization length according to the acoustical analog [15–17] drop to around four orders of magnitude from $\theta = 0.005$ to 0.78535 (please see [15, 17])! This is a clear demonstration of the effect of free orientations. Meanwhile, once the Pauli-blocking measure (B) increases or decreases from zero (Boltzmann gases), the latter (Fermi gases: $B < 0$) shows opposite trend compared to that of the former (Bose gases: $B > 0$) considering the shift of the max. λ_i state: δh. $\delta h > 0$ is for Fermi gases ($|B|$ increasing), and the reverse ($\delta h < 0$) is for Bose gases (B increasing)! This illustrates partly the interaction effect (through the Pauli exclusion principle). These results will be crucial for further obtaining the phase diagram (as the density or temperature is changed) tuned by both the free orientation and the interaction. Here, $B = -1$ or $\theta = 0, \pi/4$ might be fixed points.

To check what happens when the temperature is decreased (or h is decreased) to near $T = 0$ or $T = T_c$, we collect all the data based on the acoustical analog from the dispersion relations (especially the absorption of sound mode) we calculated for ranges in different degrees of the orientation (here, θ is up to $\pi/4$ considering single-particle scattering and binary collisions; in fact, effects of θ are symmetric w.r.t. $\theta = \pi/4$ for $0 \le \theta \le \pi/2$; cf. Chu in Ref. [15]) and Pauli-blocking measure. After that, we plot the possible phase diagram for the inverse of the rarefaction parameter vs. the orientation (which is related to the scattering) into Fig. 1 (for different Bs: $B = -0.98, -0.9, -0.1, 0, 0.1, 1$). Here, the Knudsen number (K_n) $\propto$ MFP/λ_s with MFP and λ_s being the mean free path and wave length, respectively and the temperature vs. MFP relations could be, in one case, traced from Einzel and Parpia [27] (following Fig. 3 therein). This figure shows that as the temperature decreases to a rather low value, the critical orientation will decrease sharply (at least for either Bose or Fermi gases).

In fact, qualitatively similar results (cf. Fig. 4 in [39]: therein higher relative pressure corresponding to λ_r here) show that (i) once the orientation θ increases, for the same h (or temperature; cf. [27]), the dispersion λ_r (or the relative pressure in [39]) increases (please refer to [15, 17]); (ii) as $|B|$ (B: the Pauli-blocking parameter) increases, the dispersion (λ_r) will reach the continuum or hydrodynamical limit (larger h or high temperature regime) earlier. The phase speed of the plane (sound) wave in Bose gases (even for small but fixed h) increases more rapid than that of Fermi gases (w.r.t. to the higher temperature conditions:

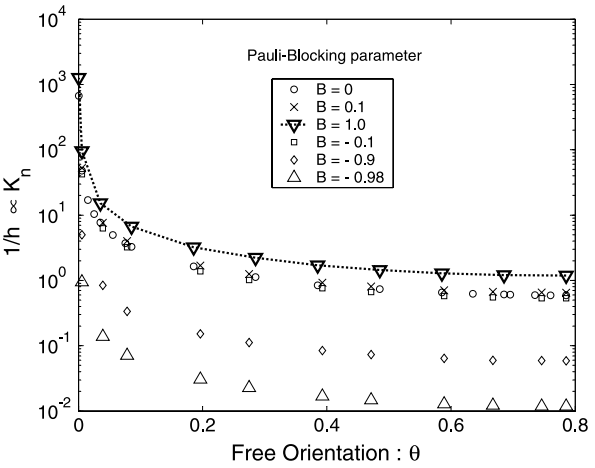

Fig. 1 Possible phase diagram for different-statistic gases w.r.t. the free orientation (θ) and Knudsen number ($K_n \propto$ the mean free path/wave length). $B > 0$: bosonic particles; $B < 0$: fermionic particles [10]. The orientation is related to either the induced scattering or internal symmetry. K_n might be transformed to the dimensionless or relative temperature (cf. Fig. 3 by Einzel and Parpia [27])

larger h) as the relevant parameter B increases. For all the rarefaction measure (h), perturbed plane waves propagate faster in Bose-particle gases than Boltzmann-particle and Fermi-particle gases (e.g., see [18–20] or [21]). In fact, the real part (λ_r) also resembles qualitatively those reported by Asakawa et al. [4] for $T > T_c$ cases.

As for the imaginary part (λ_i), there is the maximum absorption (or attenuation) for certain h (the rarefaction parameter) which resembles that reported by Broniowski and Hiller [13] (cf. Fig. 1(b) therein). We observed a jump of the (relative) sound speed in the multiple scattering case (cf. [16]) which was also reported by Tarasov [59] (at the phase transition between hadronic phase and QGP).

To know the detailed effects of interactions (tuned by the Pauli-blocking parameter: B here) and the critical orientation, which could be linked to the effective number of thermodynamic degrees of freedom (ν, for an ideal gas of massless, non-interacting constituents, ν counts the number of bosonic degrees of freedom plus the number of fermionic degrees of freedom weighted by $7/8$), we plot θ (of which the localization or resonance occurs for specific B) vs. μ (the chemical potential, in arbitrary units) in Figs. 2 and 3 by referring to two possibly localized states ($\theta = 0$ or $\pi/4$; cf. [15, 17]). The density rises from the onset of nuclear matter through the transition to quark matter as illustrated in Fig. 2. The compact star is possibly in this region of the phase diagram. Then there might be different behaviors separated by crossover regions as shown in Figs. 2 ($\theta = 0$ dominated, T (the temperature) $\propto h$ (the rarefaction measure)) and 3 ($\theta = \pi/4$ dominated, T (the temperature) $\propto 1/h$). We remind the readers that for the case of $\theta = \pi/4$ dominated (Fig. 3), as the lower temperature is associated with the higher density, fermions ($B < 0$) link to the lower temperature regime (under the same orientation).

If there are differences between ours and those reported before, it might be due to the assumption made in previous study that the matter under study is in (approximate) local thermal equilibrium. At RHIC, such evidence is believed to be provided by the agreement of the elliptic flow (cf. [41]) measured in noncentral collisions with hydrodynamic model predictions. Such predictions are based on the assumption that the matter behaves like a fluid in local thermal equilibrium, with arbitrarily short mean free paths and correspondingly strong interactions), one possible explanation could be that the assumption of a completely thermal medium is a simplification (cf. [52]). The acoustic perturbations we treated are close to the thermodynamic equilibrium (for Bose or Fermi gases). Other reasoning is related to the different types of particles (with or without fragmentation) being considered. One

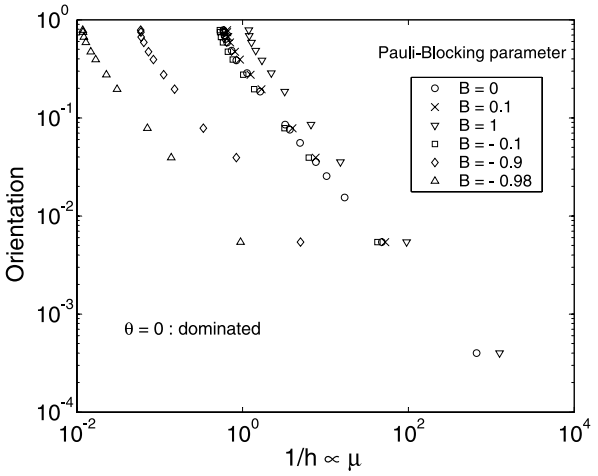

Fig. 2 Possible phase diagram for different-statistic gases w.r.t. the orientation (θ) and temperature $T \propto h$ (the rarefaction measure). The unit of μ (related to the chemical potential) is arbitrary. $B > 0$: bosonic particles; $B < 0$: fermionic particles

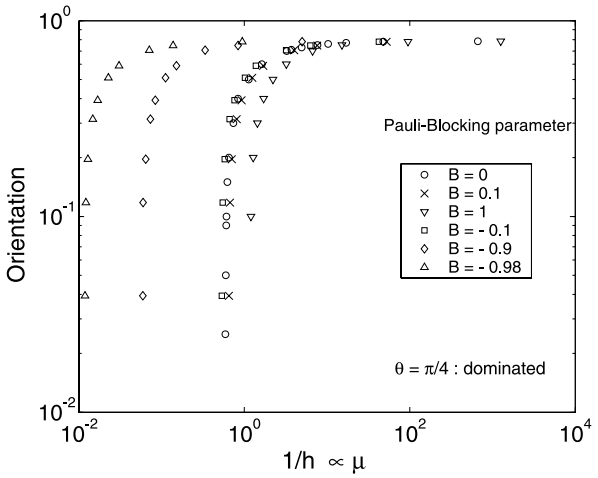

Fig. 3 Possible phase diagram for different-statistic gases w.r.t. the orientation and temperature $T \propto 1/h$ (h is the rarefaction measure and is proportional to the inverse of the mean free path; cf. Fig. 3 by Einzel and Parpia [27]). The unit of μ is arbitrary

interesting observation is that the attenuation of jet (quenching) observed at RHIC resembles qualitatively the attenuation of plane (sound) waves (cf. [15, 17]).

With above results, then our approach could provide an effective theory based on the opposite picture of very strong interaction (via the tuning of B and θ) and very small mean free paths (h is large). This can also be useful to the study of problems in astrophysics: like compact stars. For instance, one of the most striking features of QCD is asymptotic freedom: the force between quarks becomes arbitrarily weak as the characteristic momentum scale of their interaction grows larger. This immediately suggests that at sufficiently high densities and low temperatures (corresponding to the case of Fig. 3 here; cf. [15, 17] since $\theta = \pi/4$ is also possible and thus dominates the localized behavior or transition) matter will consist of a Fermi sea of essentially free quarks, whose behavior is dominated by the freest of them all: the high-momentum quarks that live at the Fermi surface.

Note that in QCD, the dominant gauge-boson-mediated interaction between quarks is itself attractive. The relevant degrees of freedom are those which involve quarks with momenta near the Fermi surface. These interact via gluons, in a manner described by QCD.

The breaking of a gauge symmetry cannot be characterized by a gauge-invariant local order parameter which vanishes on one side of a phase boundary. Considering the pairing mechanism, in conventional condensed-matter systems, where the relevant fermions are electrons, the necessary attractive interaction has been hard to find. The dominant interaction between electrons is the repulsive electrostatic force, but in the right kind of crystal there are attractive phonon-mediated interactions that can overcome it. In these materials the BCS mechanism leads to superconductivity, since it causes Cooper pairing of electrons, which breaks the electromagnetic gauge symmetry, giving mass to the photon and producing the Meissner effect (exclusion of magnetic fields from a superconducting region). The Cooper-paired state is rare and delicate, easily disrupted by thermal fluctuations, so superconductivity only survives at low temperatures. In QCD, however, the superconducting phase can be characterized rigorously only by its global symmetries. In electromagnetism there is a non-local order parameter, the mass of the magnetic photons, that corresponds physically to the Meissner effect and distinguishes the free phase from the superconducting one. In QCD there is no free phase: even without pairing the gluons are not states in the spectrum. No order parameter distinguishes the Higgsed phase from a confined phase or a plasma, so we have to look at the global symmetries (since pairs of quarks cannot be color singlets, the resulting condensate will break the local color symmetry $\mathrm{SU}(3)_{\mathrm{color}}$). Based on these, to calibrate our results (say, Figs. 2 and 3) with those obtained using the QCD, we like to remind the readers that, there is possibility about the *continuity* of quark and hadron matter, for low enough strange quark mass (via the mass spectra of quarks) there may be a region where sufficiently dense baryonic matter has the same symmetries as quark matter, and there need not be any phase transition between them! In fact, the mass spectra of particles could be inferred from the acoustic analog by using our present approach.

To conclude in brief, our illustrations here, although are based on the acoustical analog of our quantum discrete kinetic calculations, can indeed show the Fermi and Bose liquid (say, Cooper pairs) and their critical behavior for the transition (at least valid to the regime $T > T_c$ considering the QGP) once the orientation (linked to the straight string via a projection) is tuned as well as the temperature is decreased significantly. We shall investigate more complicated problems in the future (say, [8, 14, 46]) (e.g., (1) the saturated orientation shown in Fig. 3 which is almost the same for all different-statistic gases of particles might be relevant to the Stefan–Boltzmann limit; (2) the critical orientation might be related to the external strong magnetic field (cf. [18–20] or [31]) or confined potential or parameter relevant to the global internal symmetry).

References

1. Alford, M.: Dense quark matter in compact stars. In: Plessas, W., Mathelitsch, L. (eds.) Lecture Notes in Physics, vol. 583, pp. 81–115. Springer, Berlin (2002)
2. Alvarez, M.A.G., Alamanos, N., Chamon, L.C., Hussein, M.S.: nucl-th/0501084 (2005)
3. Arnold, P., Son, D.T., Yaffe, L.G.: Phys. Rev. D **59**, 105020 (1999)
4. Asakawa, M., Hatsuda, T.: Nucl. Phys. A **610**, 470 (1996)
5. Avgoustidis, A., Shellard, E.P.S.: Phys. Rev. D **73**, 041301 (2006)
6. Blaizot, J.P., Iancu, E.: Phys. Rev. Lett. **70**, 3376 (1993)
7. Blaizot, J.P., Iancu, E.: Nucl. Phys. B **557**, 183 (1999)
8. Bluhm, M., Kämpfer, B., Soff, G.: Phys. Lett. B **620**, 131 (2005)
9. Bödeker, D.: Phys. Lett. B **426**, 351 (1998)
10. Bödeker, D.: Nucl. Phys. B **566**, 402 (2000)
11. Braaten, E., Pisarski, R.D.: Nucl. Phys. B **337**, 569 (1990)
12. Braaten, E., Pisarski, R.D.: Phys. Rev. D **45**, 1827 (1992)
13. Broniowski, W., Hiller, B.: Phys. Lett. B **392**, 267 (1997)

14. Chu, W.K.-H.: J. Phys. A: Math. Gen. **33**, 7103 (2000)
15. Chu, K.-H.W.: J. Phys. A: Math. Gen. **34**, L673 (2001)
16. Chu, K.-H.W.: J. Phys. A: Math. Gen. **35**, 1919 (2002)
17. Chu, W.K.-H.: Appl. Math. Lett. **14**, 275 (2001)
18. Chu, A.K.-H.: Phys. Rev. B **70**, 174421 (2004)
19. Chu, A.K.-H.: Phys. Scr. **69**, 170 (2004)
20. Chu, K.-H.W.: (2004). Preprint
21. Chu, Z.K.-H.: (2007). Z. Angew. Math. Phys. (to be published)
22. Collins, J.C., Perry, M.J.: Phys. Rev. Lett. **34**, 1353 (1975)
23. Copeland, E.J., Kibble, T.W.B., Steer, D.A.: Phys. Rev. Lett. **97**, 021602 (2006)
24. Davis, A.C.: Contemp. Phys. **46**, 313 (2005)
25. da Silva, D.T., Hadjimichef, D.: J. Phys. G: Nucl. Part. Phys. **30**, 191 (2004)
26. Dolbeault, J.: Arch. Ration. Mech. Anal. **127**, 101 (1994)
27. Einzel, D., Parpia, J.M.: J. Low Temp. Phys. **109**, 1 (1997)
28. Elze, H.T., Gyulassy, M., Vasak, D.: Nucl. Phys. B **276**, 706 (1986)
29. Elze, H.T.: Z. Phys. C **38**, 211 (1988)
30. Gross, D.J., Pisarski, R.D., Yaffe, L.G.: Rev. Mod. Phys. **53**, 43 (1981)
31. Ferrari, L., Carbognani, A.: Chem. Phys. **215**, 37 (1997)
32. Hanany, A., Hashimoto, K.: J. High Energy Phys. **06**, 021 (2005)
33. Heinz, U.: Phys. Rev. Lett. **51**, 351 (1983)
34. Heinz, U.: Ann. Phys. (N.Y.) **161**, 48 (1985)
35. Heiselberg, H., Pandharipande, V.: Annu. Rev. Nucl. Part. Sci. **50**, 481 (2000)
36. Hindmarsh, M.B., Kibble, T.W.B.: Rep. Prog. Phys. **58**, 477 (1995)
37. Hussein, M.S., Rego, R.A., Bertulani, C.A.: Phys. Rep. **201**, 279 (1991)
38. Johnston, S., Romani, R.W.: Astrophys. J. **590**, L95 (2003)
39. Karsch, F.: Nucl. Phys. A **698**, 199 (2002)
40. Kelly, P.F., Liu, Q., Lucchesi, C., Manuel, C.: Phys. Rev. D **50**, 4209 (1994)
41. Kolb, P.F., Huovinen, P., Heinz, U., Heiselberg, H.: Phys. Lett. B **500**, 232 (2001)
42. Kotake, K., Sato, K., Takahashi, K.: Rep. Prog. Phys. **69**, 971 (2006)
43. Laine, M., Manuel, C.: Phys. Rev. D **65**, 077902 (2002)
44. Linde, A.D.: Phys. Lett. B **96**, 289 (1980)
45. Litim, D.F., Manuel, C.: Nucl. Phys. B **562**, 237 (1999)
46. Manuel, C., Tytgat, M.H.G.: Phys. Lett. B **479**, 190 (2000)
47. Manuel, C., Mrówczyński, St.: Phys. Rev. D **67**, 014015 (2003)
48. Mason, R.J. Jr. In: de Leeuw, J.H. (ed.) Rarefied Gas Dynamics, vol. 1, p. 48. Academic Press, New York (1965)
49. Maynard, J.D.: Rev. Mod. Phys. **73**, 401 (2001)
50. McLaughlin, M.A., Lyne, A.G., et al.: Nature **439**, 817 (2006)
51. Mrówczyński, St.: Phys. Rev. D **39**, 1940 (1989)
52. Müller, B.: Nucl. Phys. A **750**, 84 (2005)
53. Oppenheimer, J.R., Volkoff, G.M.: Phys. Rev. **55**, 374 (1939)
54. Polchinski, J.: Phys. Lett. B **209**, 252 (1988)
55. Sazhin, M., Longo, G., Capaccioli, M.: Mon. Not. R. Astron. Soc. **343**, 353 (2003)
56. Sazhin, M., Capaccioli, M., Longo, G., Paolillo, M., Khovanskaya, O.: Astrophys. J. **636**, L5 (2006)
57. Shellard, E.P.S.: Nucl. Phys. B **283**, 624 (1987)
58. Shellard, E.P.S., Ruback, P.J.: Phys. Lett. B **209**, 262 (1988)
59. Tarasov, Yu.A.: Phys. Lett. B **379**, 279 (1996)
60. Taylor, J.C., Wong, S.M.: Nucl. Phys. B **346**, 115 (1990)
61. 't Hooft, G.: hep-th/0408148 (2004)
62. Tolman, R.C.: Phys. Rev. **55**, 364 (1939)
63. Uehling, E.A., Uhlenbeck, G.E.: Phys. Rev. **43**, 552 (1933)
64. Vedenyapin, V.V., Mingalev, I.V., Mingalev, O.V.: Russ. Acad. Sci. Sb. Math. **80**, 271 (1995)
65. Winter, J.: J. Phys. (Paris) **45**(C6), 53 (1984)
66. Wong, S.K.: Nuovo Cimento A **65**, 689 (1970)